

A Survey of Entorhinal Grid Cell Properties

Jochen Kerdels Gabriele Peters

February 28, 2022

University of Hagen - Chair of Human-Computer Interaction
Universitätsstrasse 1, 58097 Hagen - Germany

Abstract

About a decade ago *grid cells* were discovered in the medial entorhinal cortex of rat. Their peculiar firing patterns, which correlate with periodic locations in the environment, led to early hypothesis that grid cells may provide some form of metric for space. Subsequent research has since uncovered a wealth of new insights into the characteristics of grid cells and their neural neighborhood, the parahippocampal-hippocampal region, calling for a revision and refinement of earlier grid cell models. This survey paper aims to provide a comprehensive summary of grid cell research published in the past decade. It focuses on the functional characteristics of grid cells such as the influence of external cues or the alignment to environmental geometry, but also provides a basic overview of the underlying neural substrate.

1 Introduction

The parahippocampal-hippocampal region (PHR-HF) of the mammalian brain hosts a variety of neurons whose activity correlates with a number of allocentric variables. For example, the activity of so-called *place* cells correlates with specific, mostly individual locations in the environment [50, 51], the activity of *head direction* cells correlates with the absolute head direction of an animal [66, 65], the activity of *grid* cells correlates with a regular lattice of allocentric locations [16, 22], the activity of *border* cells correlates with the proximity of an animal to specific borders in its environment [60, 59], and, finally, the activity of *speed* cells correlates with the current speed of an animal [32]. In addition, there are a number of cells whose activity reflect a combination of those variables. Together, these cells are commonly assumed to be part of a system that supports tasks of spatial representation, orientation, and navigation. Within this system grid cells stand out from the other neurons by their remarkable grid-like firing patterns that resemble a set of carefully oriented rulers spanning the entire environment. Hence, they are often seen as providing some kind of *metric for space* to the animal [46, 45].

This survey aims to provide an overview of functional grid cell properties as well as information on the underlying neuronal structures present in a major area hosting grid cells, the medial entorhinal cortex (MEC). The survey is based on previous work by one of the authors [28], but is significantly extended and

restructured to be comprehensive and self-contained. The survey is structured as follows. Section 2 introduces key measures that are widely used to identify and characterize grid cells on a functional level. Section 3 and section 4 report findings regarding the development of grid cells and their topographical organization, respectively. Section 5 constitutes the main part of this survey and covers important functional grid cell properties that were discovered within the last decade. Subsequently, section 6 turns to the underlying neural substrate reporting on findings regarding the general structure of the MEC as well as specific findings regarding possible grid cell microcircuits. Finally, section 7 concludes this survey.

2 Grid Cell Measures

Grid cells stand out from other neurons in the PHR-HF by their triangular, grid-like firing patterns. To characterize the spatial properties of this grid structure Hafting et al. [22] established four measures that are used throughout the grid cell literature: *spacing*, *orientation*, *field size*, and *phase* of a grid cell. In addition, Sargolini et al. [58] introduced a *gridness* score which quantifies the degree of spatial periodicity of a cell's firing pattern.

The basis of all five measures is the *firing rate map* of the grid cell in question. The firing rate map of a cell is typically constructed by discretizing the environment into bins of equal size (e.g. $3\text{cm} \times 3\text{cm}$) and determining the spatially smoothed, average firing rate for each bin. For instance, Sargolini et al. [58] estimate the average firing rate $\lambda(x)$ of the bin centered on position x as:

$$\lambda(x) = \sum_{i=1}^n g\left(\frac{s_i - x}{h}\right) \bigg/ \int_0^T g\left(\frac{y(t) - x}{h}\right) dt$$

with a Gaussian kernel g , a smoothing factor $h = 3$, the number of spikes n , the location s_i of the i -th spike, the location $y(t)$ of the rat at time t , and the recording period $[0, T]$. To avoid extrapolation errors bins further than the bin width apart from the tracked path of the animal are considered as unvisited. In a more recent publication, Stensola et al. [61] use a 5×5 boxcar average instead of a Gaussian kernel for smoothing. The use of this boxcar average results in firing fields that appear more accentuated and crisp compared to the Gaussian smoothing.

Four of the five grid measures, i.e., spacing, orientation, field size, and gridness require the calculation of a spatial autocorrelogram of the grid cell's firing rate map. Sargolini et al. [58] construct this autocorrelogram using the Pearson product-moment correlation coefficient $r(\tau_x, \tau_y)$ to calculate the autocorrelation between rate map bins λ separated by (τ_x, τ_y) :

$$\frac{n \sum \lambda(x, y) \lambda(x - \tau_x, y - \tau_y) - \sum \lambda(x, y) \sum \lambda(x - \tau_x, y - \tau_y)}{\sqrt{n \sum \lambda(x, y)^2 - (\sum \lambda(x, y))^2} \sqrt{n \sum \lambda(x - \tau_x, y - \tau_y)^2 - (\sum \lambda(x - \tau_x, y - \tau_y))^2}}$$

where the summation is over all n bins for which both $\lambda(x, y)$ and $\lambda(x - \tau_x, y - \tau_y)$ have valid entries in the firing rate map. Autocorrelations for shifts where $n < 20$ are not included in the resulting autocorrelogram.

Based on the autocorrelogram of the grid cell's firing rate map *spacing*, *orientation*, *field size*, and *gridness* are defined as follows. The *spacing* of a grid cell (fig. 1a) is defined as the median distance between the central peak of the

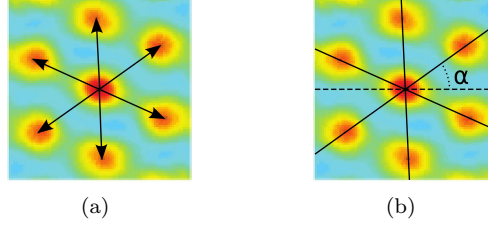


Figure 1: Grid cell spacing and orientation. (a) The *spacing* of a grid cell is defined as the median distance between the center peak and the six surrounding peaks in the autocorrelogram. (b) The *orientation* of a grid cell is defined as the angle α between a fixed reference line (dashed) going through the central peak and the closest of the three main diagonals of the grid cell hexagon in counterclockwise direction. Figures based on autocorrelogram from Sargolini et al. [58].

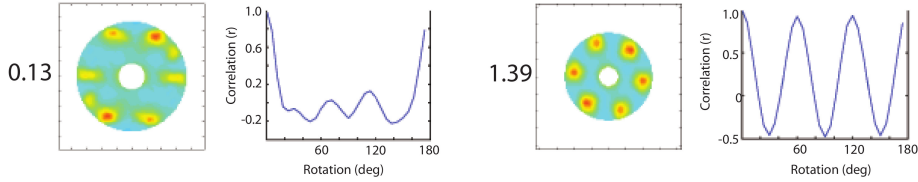


Figure 2: Gridness scores of two grid cells. The shown autocorrelograms include only the area containing the six peaks surrounding the center that was used for the calculation of the gridness scores. The graph to the right of each autocorrelogram shows the correlation of the particular autocorrelogram with a rotated version of itself in 6° steps. Gridness scores are given to the left of each autocorrelogram. Figure adapted from Sargolini et al. [58].

autocorrelogram and its six surrounding peaks. The *orientation* of a grid cell (fig. 1b) is defined as the angle between a fixed reference line (0 degrees) going through the central peak of the autocorrelogram and the closest of the three main diagonals of the surrounding hexagon in counterclockwise direction. The *field size* of a grid cell refers to the size of the individual firing fields. It is estimated as the area occupied by the central peak in the autocorrelogram with respect to a fixed threshold, e.g., $r = 0.2$ as used by Hafting et al. [22]. To calculate the *gridness score* of a grid cell only the six peaks surrounding the central peak in the autocorrelogram are taken into account. All other regions of the autocorrelogram including the central peak are masked out. Then, the correlation values between the masked autocorrelogram and rotated versions of itself at 30° , 60° , 90° , 120° , and 150° are computed. The *gridness score* is then calculated as the difference between the lowest correlation value at 60° and 120° and the highest correlation value at 30° , 90° , and 150° . Figure 2 illustrates the underlying motivation for this measure. The two graphs show the results for successive correlations between the masked autocorrelogram of a grid cell with rotated versions of itself in 6° steps. The graph shown on the right of figure 2 is an example for a grid cell with a highly periodic, triangular firing pattern resulting in high correlation values at

multiples of 60° and low correlation values in between. In contrast, the graph on the left is an example for a grid cell with a less regular firing pattern resulting in a much weaker difference between the expected correlation maxima at 60° and 120° and the expected correlation minima at 30° , 90° , and 150° . Thus, the difference between the lowest of the expected correlation maxima and the highest of the expected correlation minima provides a suitable measure of a grid cells triangular periodicity. Sargolini et al. [58] classify all cells with a gridness score greater zero as grid cells. Others, e.g., Wills et al. [69] use thresholds determined by the 95th percentile of a shuffled gridness score distribution. Typically, the shuffled distribution is obtained by randomly shifting the spike times of each cell by more than 20 seconds and less than trial duration minus 20 seconds before calculating the cell's gridness score. This way the correlation with the animal's position is broken while the temporal firing characteristics are preserved. In case of Wills et al. [69] the resulting threshold was 0.27. Hence, unlike Sargolini et al. [58] Wills et al. [69] would not classify the cell shown in figure 2 on the left as grid cell.

In contrast to the measures described so far, the *phase* of a grid cell is not an absolute measure. It describes the relative displacement between the firing grids of two co-located grid cells, i.e, grid cells with similar spacing, orientation, and field size. The relative displacement is determined by calculating the cross-correlation between the firing rate maps of the particular grid cells. Due to the cells' similarity in spacing, orientation, and field size the resulting cross-correlogram looks similar to the autocorrelogram of a single grid cell, with the main difference that the central peak is offset from the cross-correlogram's center. This offset is the relative *phase* between the two grid cells.

The previously described measures are well established and widely used across the grid cell literature. In particular, the gridness score introduced by Sargolini et al. [58] is the primary measure to identify neurons as grid cells. As a result, cells with a gridness score below the respective threshold used in a study are typically not included in the analysis. In a recent study Krupic et al. [34] introduced a different approach to characterize the firing patterns of cells in the MEA and adjacent parasubiculum (PaS). They calculated the Fourier power spectrum of each cell's firing rate map to identify the main plane waves that give rise to the firing pattern. To reduce the effects of noise they further filtered the power spectrum by subtracting the 50th percentile value of the power spectrum generated from a spatially shuffled version of the data and setting negative values to zero. Furthermore, main peaks in the vicinity of a higher peak were treated as local maxima and ignored in the subsequent analysis. To qualify as a cell with a spatially periodic firing pattern the maximal component of the Fourier power spectrum had to exceed 95% of all components in the power spectrum of shuffled data. Using this measure, it is possible to not only identify grid cells, i.e., cells with hexagonal firing patterns, but also other cells that exhibit firing patterns with a different spatial periodicity.

Krupic et al. recorded 351 cells in seven rats from layers II and III of the MEA and adjacent PaS. 65% of all recorded cells in MEA and 79% of all recorded cells in PaS were classified as spatially periodic cells. Of these 48% in MEA and 18% in PaS were classified as grid cells based on their gridness score. As expected grid cells exhibited three main components in the Fourier power spectrum which were separated by multiples of 60° . The other, non-grid cells had one to four main components with varying relative orientations and wavelengths. Figure 3

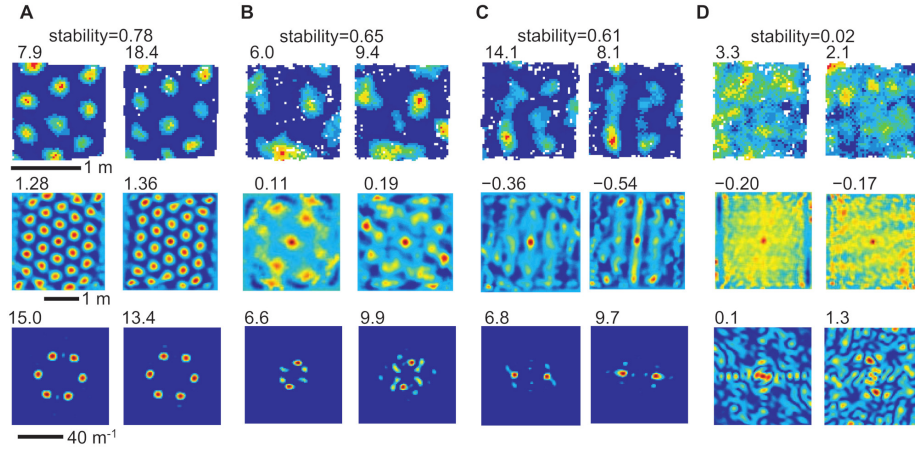


Figure 3: Examples of three spatially periodic (**A-C**) and one non-periodic cell (**D**). Data for two successive trials per cell are shown: unsmoothed firing rate maps (first row), autocorrelograms of the firing rate maps (middle row), and filtered Fourier power spectrograms (last row). Color scale from blue (low values) to red (high values). Stability of the firing patterns across trials is given as Pearson product-moment correlation coefficient between the firing rate maps. Peak firing rate, gridness score, and maximum Fourier power are indicated above the particular maps. Figure adapted from Krupic et al. [34].

shows examples of firing rate maps, autocorrelograms, and Fourier power spectra for cells with periodic and non-periodic firing patterns.

The main Fourier components of all spatially periodic cells were clustered around a limited number of orientations and wavelengths confirming the findings of Stensola et al. [61] on the topographical organization of grid cells in MEA (see section 4). In addition, the use of the Fourier spectrum revealed that the orientations of the main Fourier components of spatially periodic non-grid cells were similar to the orientations of grid cells as well and only differed in a wider distribution of relative orientations within the non-grid cells.

The firing patterns of all cells classified as spatially periodic were more stable than chance within as well as across trial days. Of these patterns the firing patterns of grid cells were the most stable. However, the number and relative orientation of the main Fourier components of some cells changed gradually over time such that, e.g., cells classified as grid cells became non-grid cells or vice versa. This change could be observed for trials within the same environment (11% of spatially periodic cells changed) as well as across different¹ environments (32% of spatially periodic cells changed). Diehl et al. [13] investigated the stability of the spatial and non-spatial firing patterns of cells in the MEA in more detail and could confirm the observations of Krupic et al. In particular, they observed that between 9% and 24% of cells in MEA depending on cell classification and environment changed their spatial firing patterns and/or firing rate across recording sessions with inter-session time intervals ranging from 5 minutes to 6 hours. In addition, they were able to characterize the change in

¹In this case “different” refers to a change from a square to a circular environment.

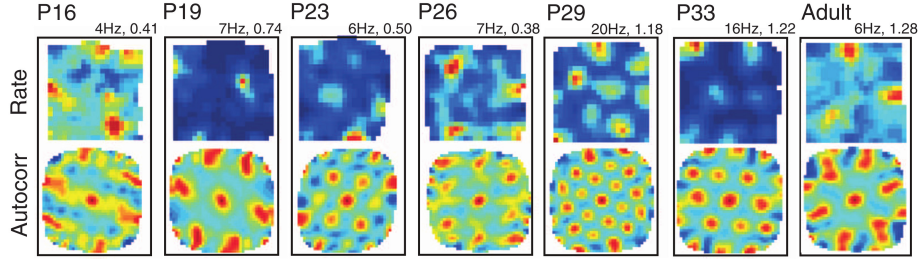


Figure 4: Firing rate maps and their autocorrelations of grid cells in rats of ages between P16 and P33. Color scale from blue (low values) to red (high values). Peak firing rates and gridness scores indicated above each rate map. Figure from Langston et al. [37].

firing patterns of individual cells as varying around a stable set point rather than random drift.

These results suggest, that grid cells may be just one instance in a continuum of spatially periodic cells [12, 13]. This hypothesis could, e.g., provide an explanation for the multi-peaked, irregular firing patterns of early, putative grid cells in developing rats observed by Wills et al. [69] and Langston et al. [37] (see next section).

3 Development

The development of spatial representations as expressed by head direction cells, place cells, and grid cells in the PHR-HF of young rats was recently investigated by Wills et al. [69] and Langston et al. [37]. Both teams used comparable experimental procedures and obtained consistent results. However, the teams differ slightly in their respective interpretations of the results.

Wills et al. [69] recorded putative place cells from CA1, as well as putative grid and head direction cells from MEA in rats between the ages of P16 (postnatal day 16) and P30. During recording the rats foraged for food in a $62\text{cm} \times 62\text{cm}$ box. Head direction cells exhibited strong directional tuning and were found in adult-like proportion right from age P16, i.e., during the rat’s first exploration of its environment². Similarly, place cells could also be observed in a significant proportion from day P16 with adult-like stability and quality in their firing pattern. Throughout the observed development period the number of place cells increased steadily towards adult-like levels. In case of grid cells, putative grid cells with multi-peaked firing fields could also be observed from day P16. However, the recorded firing patterns were irregular at first. Significant proportions of cells with adult-like, hexagonal firing patterns emerged around P20 and increased fast to near-adult proportions by P22. Based on these results Wills et al. question the hypothesis that MEA grid cells provide the only spatial input to place cells. They point out that the observed differential developmental time course suggest that the interconnectivity between grid cells and place cells develops only after the pups begin to explore their environment.

²The rat’s eyelids unseal at around P14 to P15.

Langston et al. [37] recorded putative place cells from CA1, putative grid cells from MEA, as well as putative head direction cells from pre- and parasubiculum in rats between the ages P16 and P35. In addition they recorded cells from an adult control group. During recording the rats foraged for food in a $50\text{cm} \times 50\text{cm}$ box. In essence, their observations are consistent with the results obtained by Wills et al. [69]. 61.9% of all cells recorded in the pre- and parasubiculum in rats of age P15 and P16 could be classified as head direction cells showing strong directional tuning. This proportion of HD cells was similar to the proportion found in the adult control group (64.0%). 41.4% of the recorded cells in CA1 could be classified as place cells in rats of age P16 to P18. This proportion continued to increase steadily throughout development to adult-like levels at around 60%. During development the stability of the firing fields generally increased within as well as between trials. This finding matches earlier reports on the development of place cells by Martin et al. [41]. In the MEA putative grid cells recorded in rats of age P16 to P18 showed multi-peaked, irregular firing fields. Yet, 12.8% of the cells recorded at age P16 to P18 could already be classified as grid cells. The proportion of cells passing the grid cell criterion increased slightly during development to about 17.5% in rats of age P31 to P34 being substantially lower than the proportion of grid cells measured in the adult control group ($\sim 30\%$). However, the periodic properties of cells classified as grid cells increased noticeably during development reaching gridness scores of near-adult levels at age P34. Figure 4 illustrates this development showing the firing rate maps and their autocorrelograms of several grid cells in rats of increasing age. In contrast to Wills et al. [69] Langston et al. suggest that the three observed cell types (HD cells, place cells, and grid cells) may interact from the outset of exploration. They hypothesize that the observed, rudimentary grid cells provide a sufficiently patterned input to CA1 cells to enable the generation of place-specific firing fields in the hippocampus.

4 Topographical Organization

Grid cells in the MEA are topographically organized. Neighboring grid cells exhibit similar grid spacing, field size and grid orientation, but have dissimilar phases. Starting from the postrhinal border grid spacing and field size increase along the dorsoventral axis of the MEA. A similar, systematic change of grid orientation along this axis could not be observed [22].

In order to determine the range of grid spacings and field sizes present in the MEA Brun et al. [5] recorded 143 grid cells in 15 rats that shuttled back and forth on a 18m long, linear track. The cells were sampled from all entorhinal cell layers with an emphasis on the superficial layers (layer II: 26, layer III: 35, layer II or III: 40, layers V and VI: 42) and their locations were distributed between 1% and 75% along the dorsoventral axis. To compare grid spacing and field size with respect to the cells' position the cells were grouped into a dorsal (0% - 25%, 55 cells), intermediate (25% - 50%, 59 cells), and ventral group (50% - 75%, 29 cells). Table 1 summarizes the obtained results. Grid spacing as well as field size increase from dorsal to ventral positions and, correspondingly, the number of firing fields along the 18m track decreases. In addition, an increase in field size appears to be accompanied by a reduction in peak firing rate. Grid spacing is characterized not only by median values but also by minimum values.

	dorsal	intermediate	ventral
mean number of fields	8.4 ± 0.3	5.9 ± 0.4	4.6 ± 0.4
mean field width	56.0 ± 1.0 cm	92.0 ± 6.0 cm	119.0 ± 7.0 cm
largest field width	90.0 ± 4.0 cm	129.0 ± 8.0 cm	190.0 ± 13.0 cm
minimum spacing	91.0 ± 12.0 cm	202.0 ± 24.0 cm	269.0 ± 47.0 cm
median spacing	171.0 ± 13.0 cm	301.0 ± 23.0 cm	370.0 ± 46.0 cm
mean firing rate	3.6 ± 0.2 Hz	4.5 ± 0.4 Hz	2.0 ± 0.2 Hz
peak firing rate	21.3 ± 0.9 Hz	17.4 ± 1.1 Hz	11.4 ± 0.9 Hz

Table 1: Summary of grid cell properties obtained by Brun et al. [5] for 143 grid cells in 15 rats. Cells were partitioned into dorsal, intermediate, and ventral groups according to their position along the dorsoventral axis of the MEA.

The minimum values were provided as the algorithm used to detect the firing fields missed a substantial number of visually discernable fields due to low firing rates. Thus, the median values may overestimate the true grid spacing.

Using the same experimental setup as Brun et al. [5] Kjelstrup et al. [29] could show, that the increase in grid spacing and field size along the dorsoventral axis of the MEA is reflected in the field sizes of place cells in CA3 which receive input from the MEA. The width of the place fields ranged from 1.41m in the dorsal region up to 13.59m in the ventral region of CA3.

In a recent study Stensola et al. [61] examined the topographic organization of MEA grid cells in more detail. In particular, they investigated whether the increase in grid spacing and field size along the dorsoventral axis is continuous or modular, the latter option being indicated by earlier experiments [71, 2] and theoretical considerations [42, 14]. In total 968 grid cells from 15 animals were recorded while the animals foraged in 100cm to 220cm wide, square boxes. The high number of recorded cells per animal (up to 186 grid cells) and the use of two sampling strategies that covered large parts of the MEA were key to enable the determination whether the topographic organization of grid cells is continuous or modular. In every single animal a modular organization could be observed. Grid cells within a module share similar grid spacing, field size, and grid orientation. Modules with increasing grid spacing and field size along the dorsoventral axis overlap in their extent, i.e., the positions of grid cells belonging to different modules are not separated and may interleave. Across all animals the distribution of mean grid spacing values covers a wide range with no apparent peaks. However, within animals the scale relation between grid spacings of successive modules is governed by a fixed factor of approximately 1.42 ($\sqrt{2}$) leading to a doubling of the area covered by each grid hexagon between modules. The circumstance that the same scale ratio was found in all animals despite different, absolute values for the grid spacings implies that a genetic mechanism is responsible for the scale relation while the different absolute values may be influenced or determined by external factors.

Many of the hexagonal grid patterns observed by Stensola et al. were elongated in one direction and it could be shown that grid cells sharing the same distortion

also shared grid spacing, field size, and orientation, i.e., belonged to the same module. By exploiting an experimental paradigm that provokes a *rescaling* of the hexagonal pattern in grid cells (see section 5.4), it could also be shown that grid cell modules are functionally independent. Each grid cell module exhibited the induced rescaling phenomena independent from each other, i.e., some modules exhibited rescaling while others did not. This indicates that inputs based on the same environment are processed independently by each module.

Stensola et al. found a maximum of five grid scale modules per animal and they estimate that the total number of grid cell modules in the MEA is in the upper single digit range.

5 Functional Properties

5.1 Phase Precession

The phenomenon of *phase precession* refers to a specific relation between the firing behavior of an individual neuron and the overall, extracellular activity, the electroencephalogram (EEG), of a brain region. In case of the rat hippocampus two major classes of overall, extracellular activity can be observed. Behaviors like walking, running, swimming, rearing, or jumping are accompanied by a characteristic, sinusoidal 7Hz to 12Hz activity called *theta activity* or just *theta* for short. Other behaviors like eating, drinking, or grooming, i.e., behaviors that do not change the location of the animal, correlate with large irregular activity covering a broad spectrum of frequencies. During theta activity place cells fire in bursts at specific points of the theta phase, e.g., at the trough. When an animal crosses the firing field of a place cell the point of the theta phase at which the cell fires shifts with the animal's relative position within the place field. This shift in the timing of the place cell's activity relative to the overall theta activity is called *phase precession* [52].

Hafting et al. [21] investigated whether entorhinal grid cells exhibit phase precession as well. They recorded 174 MEA grid cells from 23 rats while the rats ran back and forth on two linear tracks (235cm and 320cm, both 10cm wide). The grid cells were identified in a two-dimensional open field environment in which grid spacings ranged from 30cm to 70cm.

Grid cells in MEA layer II exhibited clear phase precession. On average grid cells started to fire at $222 \pm 62^\circ$ when the animal entered a grid field and stopped firing at $59 \pm 78^\circ$ on exit labeling the peak of the theta phase with 0° and the trough with 180° . The mean slope of a best fit linear regression line on the individual firing events of each cell was $-2.77 \pm 0.31^\circ \text{ cm}^{-1}$. In layer III of MEA 25% of all recorded grid cells showed phase precession over the complete theta cycle, another 25% showed phase precession limited to the trough of the theta-phase, and 50% exhibited no phase precession at all. On average layer III grid cells started to fire at $195 \pm 81^\circ$ and stopped firing at $192 \pm 123^\circ$ of the theta-phase. The mean slope of the linear regression line was $-0.078 \pm 0.283^\circ \text{ cm}^{-1}$.

In order to test whether the observed phase precession of grid cells is independent of signals from the hippocampus the firing phases of grid cells were recorded after inactivation of the hippocampus. This inactivation was achieved

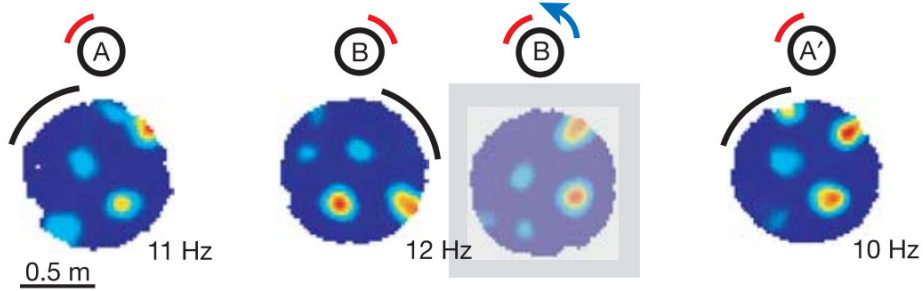


Figure 5: Anchoring of the firing pattern to an external landmark. Firing rate maps of a single grid cell recorded in a circular environment with a prominent visual cue (arc) attached to the environment’s wall. Rate maps are shown before rotation (A), after rotation by 90 degrees (B), and after counter-rotation by 90 degrees (A’). Peak firing rates are given next to the rate maps. The shaded rate map depicts the rate map of B artificially counter-rotated by 90 degrees to ease visual comparison with A and A’. Figure adapted from Hafting et al. [22].

by a local infusion of *muscimol*³, a GABA_A receptor agonist. After inactivation, the firing fields of layer II grid cells remained spatially confined, albeit the firing fields of the grid cells became wider and less stable. Theta activity and grid cell phase precession was unaffected by the inactivation of the hippocampus as well.

The question whether the phenomenon of phase precession is constitutive of grid cell firing or not is controversial [47]. A number of computational models that classify as *oscillatory interference* models use this property to explain the hexagonal firing patterns of grid cells [19]. However, experimental evidence shows that grid cell firing in bats can be observed without any sign of concurrent theta activity contradicting the prior of oscillatory interference models [74].

5.2 Influence of External Cues

Hafting et al. [22] were the first to characterize basic functional properties of grid cells. One of the key questions they address in this work is whether the locations of grid cell firing fields are determined by external landmarks (allothetic cues) or internal information about the rat’s movement (idiothetic cues). They found that the firing fields of grid cells stay constant across successive exposures to a single environment indicating a strong influence of allothetic cues. To further investigate a possible anchoring of the firing fields to external landmarks 24 grid cells in the dorsocaudal region of the medial entorhinal cortex (dMEC) in three rats were recorded. While the rats chased food pellets in a circular environment, a prominent visual cue at the wall of the environment was rotated by 90 degrees. The grid orientation of all 24 grid cells followed this rotation and only returned to their original alignment when the visual cue was counter-rotated to its original position (fig. 5).

Despite this strong influence of allothetic cues on the orientation and phase of the grid cell firing fields external cues are not necessary to maintain the firing pattern itself. Hafting et al. demonstrated this property by recording the activity

³5-aminomethyl-3-hydroxyisoxazole

of grid cells (4 rats, 33 cells) in total darkness (30 minutes) preceded by a period of regular illumination (10 minutes). Besides a weak dispersal of the firing fields the overall grid pattern stayed intact during the period without illumination. Hafting et al. conclude that these findings indicate that the grid pattern itself may result to a large extent from hardwired network mechanisms, but that the particular alignment of the pattern is determined by external landmarks. Kraus et al. [31] investigated the maintenance of the grid pattern based on idiothetic cues and elapsed time further. They recorded grid cells while rats were running on a motorized tread mill and could observe that grid cells were able to integrate elapsed time as well as the distance that the animals had run.

5.3 Realignment

A similar influence of external landmarks as described in the previous section was already known to apply to hippocampal place cells [51], i.e., a rotation of visual cues results in a corresponding rotation of a place cell's firing field. Likewise, the firing pattern of a place cell remains intact during locomotion in darkness. Further investigation of the influence of distant visual cues on place cell activity revealed the phenomenon of *remapping* [49, 48]. For a given environment a certain set of place cells represents this particular environment. When the environment changes, e.g., when a rat is placed from one experimental environment into another, a different set of place cells gets recruited to represent the new environment. This switch from one set of place cells to another is termed *global remapping* [38, 26] and it only occurs if the environment changes significantly. If, in contrast, the environment changes only slightly, the same set of place cells is used but the maximum intensity with which individual place cells are active changes. This change of maximum activity is termed *rate remapping* [38].

Given the similar behavior of grid cells and place cells with respect to the influence of external landmarks, Fyhn et al. [15] investigated how grid cells would behave during environment changes that reliably induce either *global remapping* or *rate remapping* in hippocampal place cells. Global remapping was induced by three protocols: switching between a square and a circular environment at a fixed location in one room, switching between similar square environments in two rooms with different background cues, and switching between light and darkness in a single, square environment. Rate remapping was induced by a single protocol in which the colors of the walls of a single, square environment were changed. Neuronal activity was recorded in dorsocaudal MEA and/or dorsal CA3 in 19 rats. The protocols reliably induced global and rate remapping in all trials in which CA3 place cells were recorded.

Global remapping induced by the first protocol, i.e., alternating between square and circular environments, led to an absolute shift of the grid up to one-half grid spacing while the distributions of grid spacing, grid orientation, and relative phases were preserved (fig. 6A). The directions of the grid shifts were uniformly distributed across experiments. However, for individual cells that were recorded over several days the direction and magnitude of the grid shift remained constant. The second protocol, constituting a stronger environment change, led not only to a shift of the grid pattern but also to a grid rotation (fig. 6B). Additionally, in some cases (three out of seven for the first protocol, five out of eight for the second protocol) the overall grid spacing slightly scaled between

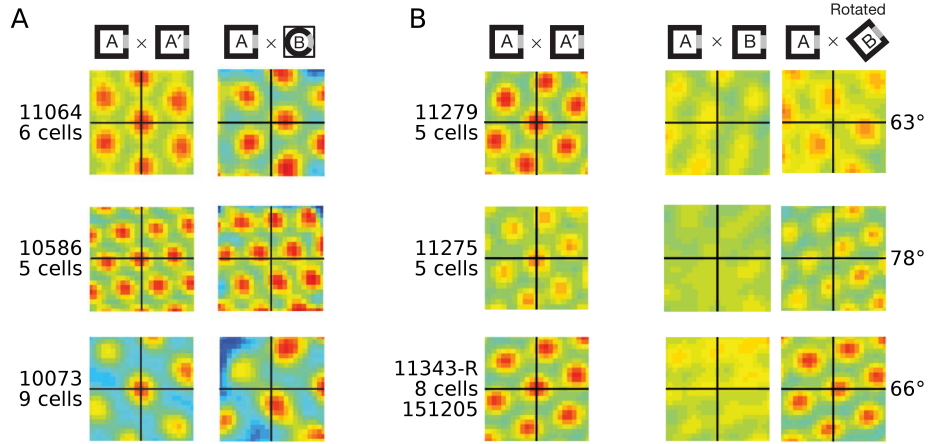


Figure 6: Illustration of grid cell realignment. The maps show cross-correlations of firing rate maps for small populations of grid cells (5 to 9 cells) in individual animals (5-digit numbers). **A**: Switching between a square and circular environment causes a shift of the grid pattern while spacing, orientation, and relative phases are preserved. **B**: Switching between square environments located in different rooms causes not only a shift of the grid pattern but also a rotation of the pattern. The angle of rotation was determined by successively rotating the firing rate maps of environment B until the resulting pattern in the cross-correlogram had maximal grid structure. Figure adapted from Fyhn et al. [15].

environments. These results indicate that grid cell ensembles do not change during global remapping and instead perform a *realignment* of grid orientation and position. They further suggest, that the relative phases of grid cells within a local ensemble may be in a rigid relationship (this hypothesis was recently supported by results of Yoon et al. [75]). The third global remapping protocol was used with two rats that had electrodes in MEA as well as CA3 to determine whether grid cell realignment and place cell remapping are coincident. In one animal global remapping of place cells coincided with an equally fast grid cell realignment, whereas in the second rat place cells and grid cells maintained their firing fields after a switch from the dark to the light condition. In the latter case, global remapping and realignment could be triggered by temporarily interrupting the movement of the rat by placing it for one minute on a pedestal. Fyhn et al. argue that this delayed remapping reflects a continued influence of self-motion information on the location of place cell and grid cell firing fields.

Contrary to the global remapping condition no change of grid cell activity could be observed during rate remapping. The results obtained by Fyhn et al. suggest two main implications. First, as the ensemble of grid cells and their relative, spatial relationship does not change across environments, similar paths of an animal in different environments are mapped onto similar sequences of grid cells supporting the hypothesis that grid cells are part of an universal metric for path-integration-based navigation. Second, as hippocampal CA3 receives both direct and indirect input from the MEA the realignment of grid cells could serve as a basis for the remapping occurring in hippocampal place cells [44].

A number of recent publications provide further insight into the relations

between MEC and hippocampus. Zhang et al. [76] used a combined optogenetic-electrophysiological strategy to map out the functional inputs to hippocampal place cells that originate in the entorhinal cortex. Their main finding suggests that hippocampal place cells receive input from a wide variety of functional cells in the MEC including grid cells, border cells, head direction cells, irregular spatial cells, and non-spatial cells. Miao et al. [43] investigated the influence of partial MEC inactivation on hippocampal place cells. They induced the partial inactivation by a pharmacogenetic approach and could observe hippocampal remapping in CA3 as response. The inactivation did not influence the shape or size of the observed place fields, but their distribution at the ensemble level changed significantly. Importantly, this remapping took place almost instantaneously. In contrast, Rueckemann et al. [57] performed a similar experiment, but observed a slow and lasting change in the place cell ensemble after a partial inactivation of MEC. However, Rueckemann et al. used an optogenetic instead of a pharmacogenetic strategy to partially silence the MEC and, more importantly, they observed hippocampal place cells in CA1 instead of CA3. These differences in the experimental setup may explain the diverging results regarding the time course of the observed remapping. Marozzi et al. [40] explored the effects of non-metric context changes, i.e., changes in color and smell of the environment on grid cell firing patterns and could observe a realignment of the grid phase as response. Finally, Olafsdottir et al. [53] addressed the question if and how the activity of grid cells is involved in the well known phenomenon of *hippocampal replay*. They recorded grid cells in layers V and VI of the MEC and could show that these cells were spatially coherent with hippocampal place cells during replay. The grid cells encoded the particular locations with a 11ms delay, indicating monosynaptic feedback connections from hippocampus to layers V and VI of MEC.

5.4 Rescaling

The slight scaling effects observed by Fyhn et al. [15] during realignment can have a much larger magnitude under certain circumstances. Barry et al. discovered and investigated these stronger *rescaling* phenomena in two different contexts [2, 1].

The first context in which a significant rescaling of grid cell firing patterns can be observed is the geometric deformation of a known environment [2]. Barry et al. trained six rats to be accustomed to either a square ($1m \times 1m$, 3 rats) or a rectangular ($0.7m \times 1m$, 3 rats) environment. Subsequently, the trained rats were exposed to scaled versions of these environments while the activity of MEA grid cells was recorded. The square (s) and rectangular (r) environments were scaled horizontally ($s : 0.7m \times 1m \mid r : 1m \times 1m$), vertically ($s : 1m \times 0.7m \mid r : 0.7m \times 0.7m$), and in both directions ($s : 0.7m \times 0.7m \mid r : 1m \times 0.7m$). In all cases the recorded firing patterns of the grid cells showed strong rescaling in the direction in which the particular environment was scaled, though with a lesser magnitude (fig. 7). Re-exposure to the unscaled, familiar environment (Trial 5) showed, that the rescaling effect is not permanent. On average grid patterns rescaled by 47.9% with respect to the change of the environment. In addition, cases of uni-directional scaling, i.e., in either horizontal or vertical direction, were accompanied by a small, opposite rescaling (7.9% on average) of the grid patterns in a direction orthogonal to the change of the environment.

Barry et al. hypothesize that environmental features like boundaries become

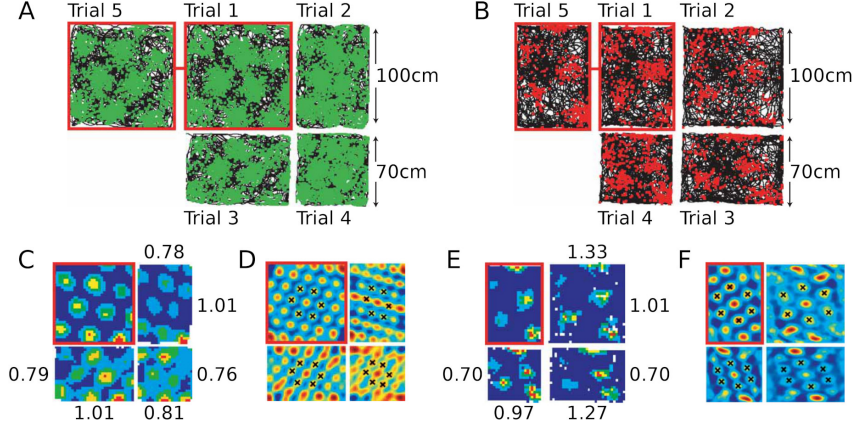


Figure 7: Illustration of grid cell rescaling. **A,B**: Firing events (green and red dots) of single grid cells superimposed on the path (black lines) of two rats in scaled environments. Trials 1 and 5 took place in the environment to which the rats were accustomed to (red outline). **C,E**: Color-coded (blue: low, red: high) firing rate maps. Grid scaling for each dimension indicated by numeric labels. **D,F**: Color-coded autocorrelograms of the firing rate maps. Peaks of the central hexagons are marked with black crosses. Figure adapted from Barry et al. [2].

associated with the grid pattern over time, such that a sudden deformation of the environment causes a corresponding deformation of the grid pattern. However, with an increasing number of trials, grid patterns in the changed environment rescaled with lower and lower magnitude indicating that rescaling is not solely a reflection of the environment’s changed geometry but also a reflection of the animal’s increasing familiarity with the modified environment. Barry et al. suggest that this reduction in rescaling reflects a tendency of the grid cells to revert to an intrinsic grid scale.

The second context in which rescaling of grid cell firing patterns was observed is exposure to novel environments [1]. In the corresponding study MEA grid cells of eight rats were recorded while the animals foraged in $1m \times 1m$ environments. The rats underwent five trials (20 minutes each) per day for up to seven consecutive days. Each day, the rats were first exposed to a familiar⁴ environment, followed by three novel environments, and finally the familiar environment again. Novel environments differed in texture, visual appearance, and odor. Exposure to the first novel environment on the first day caused realignment (rotation and shift) as well as rescaling of all recorded grid patterns. On average the grid patterns scaled up by 37.3% (min.: 10.5%; max.: 71.1%). In addition, the average gridness score dropped from 0.65 in the familiar environment to 0.04 in the novel environment as the hexagons of the grid patterns were less circular in the novel environment. Exposure to the second and third novel environment resulted in rescaling with less magnitude, i.e., grid patterns in the fourth trial scaled up 21.3% on average. This trend continued over subsequent days. On the

⁴familiar := a minimum of 100 minutes of prior exposure

second day the average increase was 16.2% and on day five no grid cell showed any discernable rescaling. In some cases the firing pattern of individual grid cells already showed no apparent rescaling after three days.

In order to examine if place cell remapping co-occurs with grid cell rescaling another seven rats were implanted with electrodes recording simultaneously in MEA and CA1. The rats were tested by a similar protocol as described before, yet the environments used were not identical. Upon first exposure to a novel environment the firing patterns of the recorded grid cells scaled up by 33.9% on average, and the average gridness score decreased from 0.96 to 0.31. Simultaneously recorded place cells showed an immediate and complete remapping and the average size of place fields in the novel environment increased by 28.8%. Furthermore place fields in the novel environment appeared to be less stable and more fraying. A subsequent weakening of grid pattern rescaling in the second and third novel environment could be observed as well (trial 3: 14.6%; trial 4: 16.8%) and was accompanied by a similar, though smaller decrease of place field scaling (trial 3: 11.3%; trial 4: 7.6%⁵).

In summary these results show that in novel environments the firing patterns of grid cells as well as place cells expand and become less regular. With increasing exposure to the new environments the firing fields of grid cells and place cells reacquire the properties seen in familiar environments, i.e., they become more regular and smaller in spatial scale. As a further mechanism that may underlie these rescaling phenomena Barry et al. propose a possible influence of the neuromodulator acetylcholin (ACh) which is implicated in novelty detection. This hypothesis is supported by the fact that co-recorded grid cell patterns scale up by similar amounts.

5.5 Influence of Environmental Geometry

The phenomena described in the previous sections were further investigated by Krupic et al. [33]. In contrast to previous reports they could show that environmental geometry can have a lasting influence on the firing patterns of grid cells. In a first experiment they demonstrate that the geometry of the experimental arena can control grid orientation and override the influence of prominent distal cues if the geometry is *polarized* as, e.g., in the case of a square environment. If such an experimental enclosure is rotated 45°, the grid orientation follows this rotation (mean grid rotation $42.5^\circ \pm 2.9^\circ$) despite the presence of stationary distal cues. However, if the enclosure is rotated 90°, the grid orientation remains unchanged (mean grid rotation $1.1^\circ \pm 0.9^\circ$). The latter case indicates that other local cues like smells or textures do not influence grid orientation. Further investigation (275 grid cells, 41 rats) showed that grid orientation aligns to the walls of square enclosures at a mean angle of $8.8^\circ \pm 0.6^\circ$ while the results for unpolarized environments were less clustered. As one consequence of this alignment the relative orientation between different grid cell modules should be either 0° or 30° in square environments due to the 60° symmetry of the grid pattern in relation to the 90° angles of the environment. Apart from a few intermediate values the observed relative orientations confirmed this hypothesis. Yet, these relative orientations remained stable in circular and hexagonal environments as well indicating that anatomically close grid cell

⁵This measurement did not reach a significance level of 0.05 (0.07).

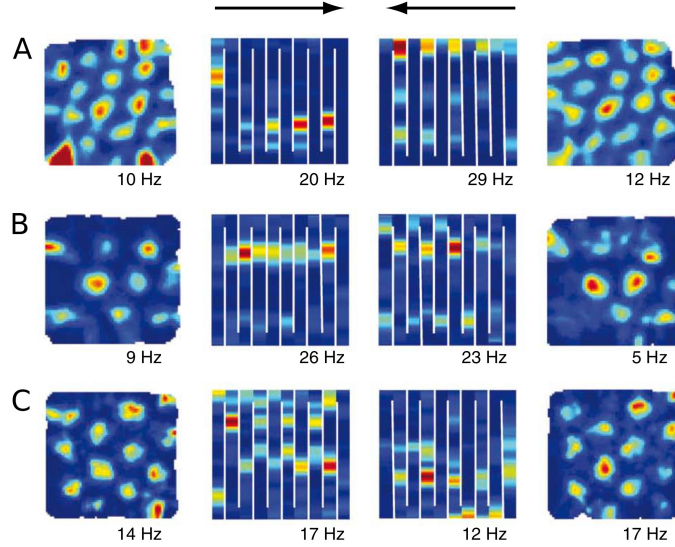


Figure 8: Firing rate maps of three grid cells (rows A, B, C). Firing rates are represented by blue (low) to red (high) colors. Peak firing rates are given below the maps. The first and last columns show the firing rate maps in the open-field, while the second and third columns show the firing rate maps in the hairpin maze according to the animal’s running direction (indicated by black arrows). Figure adapted from Derdikman et al. [11].

modules can act coherently across different environments. The findings of Krupic et al. regarding the alignment of grid orientation to enclosure walls matches the findings of a similar study by Stensola et al. [62]. The latter hypothesize that the alignment might be a way to minimize symmetry with the borders of the environment.

Krupic et al. also repeated the rescaling experiments of Barry et al. [2] described above, but they switched from a square to a trapezoid environment instead of a rectangular one. Their observations matched those of Barry et al. as firing fields expanded in response to the novel environment. Yet, contrary to the observations of Barry et al. this expansion reduced only slightly afterwards and firing fields remained 20% to 30% larger compared with the firing field sizes in a concurrently recorded square environment. In addition, grid patterns in the trapezoidal enclosure showed a permanent decrease in gridness score due to more elliptical, hexagonal patterns and less evenly distributed firing fields. Based on these results Krupic et al. conclude “that most assumptions about the invariant nature of grid cell firing are invalid” and that “in particular the role of environmental boundaries has been underestimated”.

5.6 Fragmentation

The phenomena of realignment and rescaling of grid cell firing patterns were observed and examined in rectangular or circular environments in which the rats could move around freely without encountering any obstacles. However, real environments are more likely to consist of multiple, connected subenvironments.

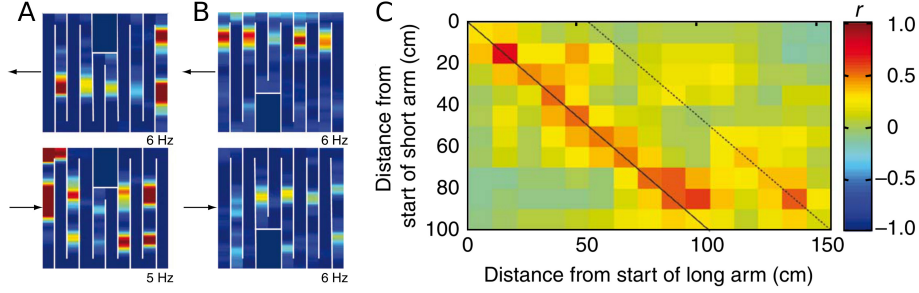


Figure 9: Modified hairpin maze with two arms shortened by 50cm. **A,B**: Firing rate maps of two grid cells recorded in a modified hairpin maze. Firing rates are represented by blue (low) to red (high) colors. Peak firing rates are given below the maps. The animal’s running direction is indicated by black arrows. **C**: Correlation between the activity (10cm bins) in a short arm with the mean activity (10cm bins) in the corresponding long arms. Figure adapted from Derdikman et al. [11].

To investigate whether grid cells exhibit a continuous or fragmented firing pattern across such subdivided environments Derdikman et al. [11] recorded MEA grid cells of rats that ran through a hairpin maze consisting of several corridor-like passages connected by sharp, 180° turns (white bars in fig. 8). The experimental protocol consisted of four consecutive, twenty minute trials per day. In the first and last trial each rat foraged in an open-field box ($1.5m \times 1.5m$). In between, i.e., in the second and third trial, each rat ran back and forth in a hairpin maze which was inserted into the open-field box. A total of 105 MEA grid cells in 16 rats were recorded.

Within this experimental setup grid cells showed the expected triangular firing pattern in the open-field box and lost this pattern in the hairpin environment (fig. 8). In the hairpin environment the firing fields of grid cells were located at similar positions in individual maze arms relative to the rats running direction, i.e., firing fields in maze arms with equal running directions had similar positions while firing fields in maze arms with opposite running directions had differing positions in general. This result suggests that grid cell firing patterns reset at the turning points of the hairpin maze. To test whether the firing fields were anchored to the preceding or upcoming turning point, two arms of the hairpin maze were shortened by 50cm (fig. 9). The resulting firing activity of each shortened arm was correlated with the activity of all corresponding long arms using 10cm wide bins and a progressive shift of the short arm to cover any possible alignment. Figure 9C shows exemplarily the correlogram of one short arm with the mean activity of all corresponding long arms. In general, the short arm correlates more strongly with the longer arms if it is aligned to the preceding wall, i.e., the activity pattern within a short arm is more similar to the start of a long arm than to its end with respect to the shared wall. However, the end of the short arm also correlates to some degree with the end of the long arms, i.e., when aligned to the upcoming wall. Together, these results indicate that the location of the firing fields is possibly determined by two mechanisms: in part by a form of path integration after a turning point, and in part by some form of environment-based alignment towards the upcoming turning point.

To exclude the possibility that the observed firing patterns could be caused by the running pattern of the animals, the rats were trained to run the path of the hairpin maze in the open-field environment without the presence of the maze walls. The observed grid cell firing pattern matched the firing pattern during the random foraging task in the open-field box. Thus, excluding a behavioral cause for the fragmentation seen in the hairpin maze.

Derdikman et al. examined also whether the observed resetting of the grid cell firing fields would influence hippocampal place fields. They recorded 111 place cells in CA3 (4 rats) and 47 place cells in CA1 (3 rats) and recorded their activity using the same experimental protocol as above. Place cells recorded while the animal was in the hairpin environment showed a fragmentation of their firing fields similar to that of grid cells. Place fields in arms with the same running direction were highly correlated, whereas place fields in arms with different running direction were only weakly correlated. This co-occurring fragmentation of MEA grid cell firing fields and CA1/CA3 place fields is another indication for a possible coupling between the spatial representations in the MEA and the hippocampus.

The observations made by Derdikman et al. [11] and Krupic et al. [33] suggest, that contrary to prior assumptions grid cell firing may primarily be determined by local environmental cues instead of forming a single, global representation of the environment. To test this hypothesis Carpenter et al. [10] devised an experiment where rats foraged in two perceptually identical enclosures connected by a corridor (fig. 10a). The walls of the environment were painted black and distal cues were hidden by black curtains. Lighting was provided by two single lights on the south wall of each enclosure. To control for other sensory cues such as odor, which could help the animal to distinguish between the compartments, the floor was rotated, the compartments swapped, and the environment cleaned in the middle of each recording session, i.e., each session consisted of a 40 minute trial (Trial 1), then the reconfiguration and cleaning of the environment, and a second 40 minute trial (Trial 2).

To determine if the firing pattern of a grid cell would locally replicate in each compartment or if it would globally cover both compartments, Carpenter et al. fitted a local and a global model to the firing rate map. In case of the local model the fitted grid had the same orientation, scale, and phase in both compartments. In case of the global model the fitted grid covered both compartments, i.e., the phase remained continuous across compartments. During the first recording sessions, the firing rate maps of the recorded grid cells (85 cells, 8 rats) were best described by the local model confirming the observations of Derdikman et al. and Krupic et al. described above (top row in fig. 10b). However, with prolonged exposure to the environment, the fit of the local model steadily decreased while the fit of the global model increased, i.e., the observed grid cells formed a global instead of a local representation of the environment with experience (bottom row in fig. 10b). The transition from a local to a global representation appeared to occur gradually and continuously. In particular, Carpenter et al. were able to track the adjustment of the firing fields of a single grid cell over a prolonged period of time observing that the firing fields “appeared to shift continuously, rather than undergo a sudden transformation”.

Wernle et al. [68] conducted a similar experiment in which rats were first trained to forage for food in two adjacent environments A and B that shared common distal cues and were separated by a central wall. After training the

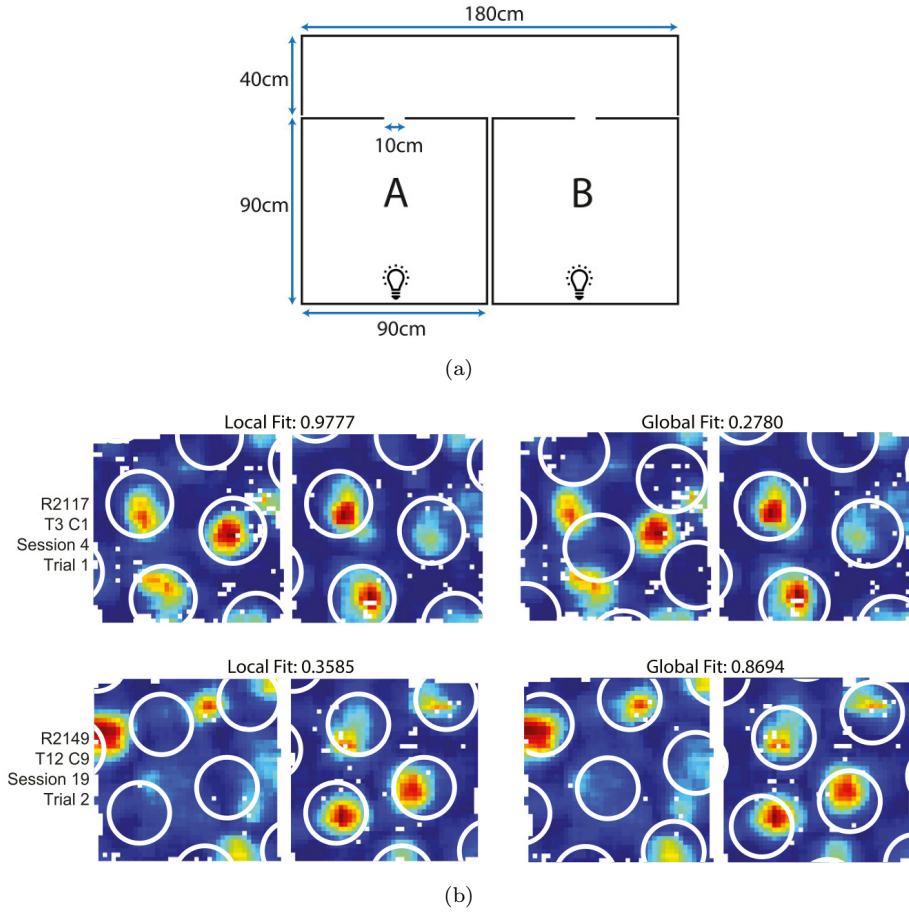


Figure 10: Prolonged exposure to an environment can lead to a global representation in grid cells. **(a)** Schematic of the experimental setup. Two perceptually identical environments A and B were connected by a corridor. **(b)** Example of two firing rate maps (rows) fitted to a local and a global model (columns). The rate map from an early session (top row) was better explained by the local model, whereas the rate map from a late session (bottom row) was better explained by the global model. Figures adapted from Carpenter et al. [10].

rats were then exposed to the joint environment AB by removing the separating wall. Wernle et al. recorded 128 grid cells (10 rats) that were active in all three environments (A, B, and AB). In agreement with the observations of Carpenter et al. the majority of the grid cells represented the environments A and B with separate grid patterns that differed in phase, and occasionally also in orientation and scale. After removal of the central wall the separate grid patterns merged into a single, locally coherent grid pattern. In contrast to the observations of Carpenter et al. this reorganization of the grid pattern happened on a fast time scale, i.e., within minutes during the first trial in the joint environment. Furthermore, Wernle et al. report that firing fields near the outer borders of the joint environment remained anchored to their positions during reorganization

while firing fields near the removed central wall moved away from their original locations in order to self-organize into a locally coherent grid pattern.

In summary, these results indicate that the early hypothesis of *stable* grid patterns that span the entire environment and serve as a metric for space [46, 45] has to be revised to reflect these more recent observations of dynamic changes in grid cell firing patterns and their anchoring to environmental cues. Carpenter and Barry [9] provide a first discussion in this regard.

6 Neuronal Structure

Neurons with grid-like firing patterns were found in all populated layers of the MEA [22, 58] as well as the PrS and PaS [3] (see Tang et al. [64] for a recent contradictory report on layer III). Interestingly, the subsequently described morphology of neurons found in these layers is not homogeneous, i.e., grid-like firing patterns are exhibited by cells with varying morphologies [56, 20]. It is an open question whether grid patterns are generated independently by various types of cells or by just a single cell type which then projects a grid signal to other cells that merely forward the signal.

6.1 Neuron Morphology in the Entorhinal Cortex

The entorhinal cortex is the origin of a prominent pathway, the *perforant path*, that connects the EC with all regions of the hippocampus. In addition, the EC receives inputs from various regions of the brain including the neocortex [72]. As a consequence, the EC is commonly thought of as the gateway to the hippocampus. As such the neuronal structure of the EC has been extensively studied even before the discovery of grid cells. If not noted otherwise the neuronal structures reported below refer to the rat brain. As the PHR-HF is constantly present in all mammalian species with little variation during its phylogenetic development, insights into the neuronal structures of rat EC can be generalized to other mammalian species, e.g., humans to a certain degree [25]. The following paragraphs will briefly summarize the key morphological properties of principal neurons found in the EC layer by layer and provide an overview of other structural properties like local microcircuits and indications of a possible columnar organization of the EC.

The overall structure of the EC comprises six layers. Layers I to III are referred to as *superficial* layers whereas layers IV to VI are referred to as *deep* layers. Layer I contains only few neuron soma and is mainly occupied by dendritic and axonal processes originating from cells located in lower layers. Layer II is densely populated by stellate cells and small pyramidal cells as its principal neurons [39]. In LEA layer II splits into Layers IIa and IIb. Layer IIb is a continuation of MEA layer II whereas layer IIa is located more superficially and consists of stellate cells forming local clusters or “islands” [35]. The principal cells of layer III are mostly pyramidal cells. Layer III is relatively thick and is followed by cell poor layer IV which contains only sparsely scattered pyramidal cells. The relatively thick layer V hosts mostly small pyramidal neurons [39]. Both layer IV and layer V are thicker in LEA than in MEA due to a higher neuron count and a less dense packaging of the cells in LEA [35]. The principal cells of layer VI are mainly globular and polygonal cells [39].

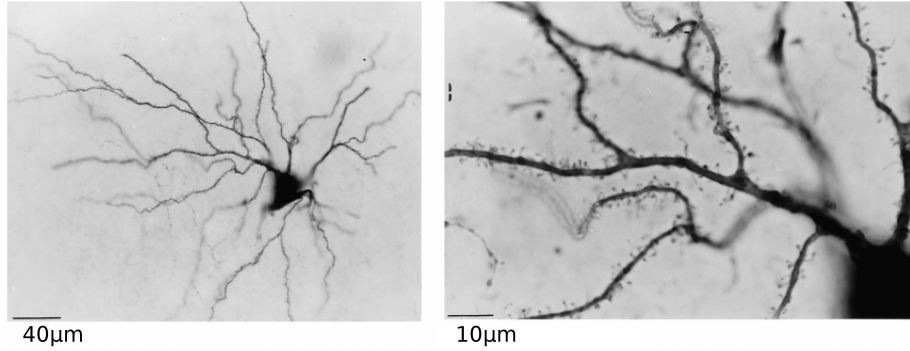


Figure 11: Photomicrograph of a stellate cell in layer II of the MEA. **(left)** The numerous primary dendrites taper gently and remain relatively thick far from the soma. **(right)** Image section showing thick dendrites covered evenly with spines. Figure adapted from Klink and Alonso [30].

6.1.1 Layer II

The principal neurons in EC layer II are of stellate and pyramidal morphology. In addition, small numbers of neurons with fusiform, horizontal tripolar, and bipolar shapes were found. The distribution of the two main neuron types, stellate cells and pyramidal cells, is not uniform between LEA and MEA. In the latter stellate cells are more abundant and pyramidal cells are mostly found near the layer III border [30].

The stellate neurons in layer II have triangular, rectangular, or trapezoidal cell bodies [39]. They possess several thick, primary dendrites which decrease in numbers dorsoventrally from an average of ten down to seven (max. 14, min. 5) [17]. The average ratio of primary dendrites to the number of dendritic endpoints is about 1:15 (min. 1:10.8, max. 1:24.7) and measurements of the overall dendritic length range from 12.8mm to 18.1mm [39]. Reports on the shape of the dendritic domain vary. Lingenhöhl and Finch [39] report a spectrum of shapes from circular domains with centrally located soma to broad, ellipsoidal domains with marginally located soma. Klink and Alonso [30] describe double V-shaped, bi-triangular dendritic domains. Others refrain from characterizing the overall, general shape of the dendritic domain [18, 54, 7]. In general the apical dendrites of stellate cells branch profusely in layer II and layer I and reach up to the pial surface [18, 39, 30, 54]. The basal dendrites extend within layer II and superficial regions of layer III [30, 54]. In some cases basal dendrites extend down to layer IV [39]. The entire dendritic tree of the stellate cells in layer II is evenly covered by dendritic spines (fig. 11) with an estimated 0.5 to 1 spines per $1\mu\text{m}$ [39]. Considering an overall dendritic length of about 15mm leads to an estimate of 7500 to 15000 spines per stellate cell where each spine can host one or more synaptic connections. The stellate cell's axon gives rise to about three to five axon collaterals within its first $400\mu\text{m}$. The axon collaterals are oriented towards the superficial layers, branch repeatedly, and form a "delicate net over the entire dendritic domain" [30]. A number of long axons branches extend parallel within layer I in mediolateral direction beyond the cell's dendritic field [30, 54]. Additionally, axon collaterals spawning in deep portions of layer III

and in layers IV to VI were also observed [30].

Pyramidal neurons in layer II have one or two apical dendrites that start to branch at the border between layer II and layer I. Secondary dendrites appear to branch off almost perpendicular resulting in a bitufted appearance of the dendritic arbor [18, 30]. The basal dendrites of layer II pyramidal cells branch extensively around the soma and are confined to layer II and the upper parts of layer III. The density of dendritic spines is higher in comparison to stellate cells, especially in case of the apical dendrites [30]. The ratio of primary dendrites to the number of dendritic end points was measured in one case to be 1:9.4 [39]. The axon of layer II pyramidal cells is thin and meanders through layer II, III, and IV giving off several, mainly horizontal collaterals that branch multiple times. Some collaterals ascend to upper layers [18, 30]. The main axon continues on a radial path towards the angular bundle⁶ (AB) [30].

6.1.2 Layer III

The principal neurons of EC layer III are pyramidal cells with a prominent, triangular cell body and radially extending primary dendrites. The apical dendrites of large pyramidal cells bifurcate in layer III and extend further into layer II and layer I where they continue to branch. Smaller pyramidal cells do not bifurcate but still extend into layer II and layer I. Basal dendrites branch extensively in layer III, but extend to deep layers as well. All dendrites of layer III pyramidal cells are densely covered with spines [39, 54]. Lingenhöhl and Finch report of up to five primary dendrites with an average ratio between primary dendrites and the number of dendritic endpoints of about 1:12 (min. 1:11.2, max. 1:15.5) [39]. In the same study the total dendritic length of a big pyramidal neuron was measured to be 11.3mm and the corresponding length of a small pyramidal neuron was measured to be 6.6mm. The axon of layer III pyramidal cells gives off several collaterals already within layer III which either extend parallel to the layer along the anteroposterior axis or extend towards the superficial layers where they stay restricted to the region occupied by the dendritic domain of the cell. Further collaterals of the axon branch off in layer V. Compared to the axons of layer II neurons, the axonal branches of layer III pyramidal cells appear to be distributed more evenly [54].

6.1.3 Layer IV

Layer IV of the EC is commonly regarded as virtually devoid of neurons. However, Lingenhöhl and Finch [39] managed to sample a number of sparsely scattered regular-sized and large-sized pyramidal cells as well as one spindle cell in this layer. The larger pyramidal cells and the spindle cell were located at the border to layer V. The regular-sized pyramidal cells ($n = 3$) had between six and eleven primary dendrites with an average ratio between primary dendrites and the number of dendritic endpoints of about 1:9 (min. 1:7.4, max. 1:10.1). The total dendritic length of one cell was estimated to be 8.3mm. The basal dendrites branched predominantly in layer IV and layer V with a few dendrites reaching up to deep portions of layer III. The apical dendrites extended into layer II and layer I where they ramified. On their way up they bifurcated already in layer IV without any further bifurcation in layer III, leaving the latter essentially free of

⁶The angular bundle lies below layer VI.

layer IV dendrites. Spines were present on all parts of the dendritic tree. The larger pyramidal cells ($n = 2$) at the border to layer V had five and eight primary dendrites, respectively with ratios between primary dendrites and the number of dendritic endpoints of 1:11.2 and 1:8.8. The total dendritic length was measured as 13.0mm and 13.3mm. In general the dendritic domains were similar to that of the regular-sized pyramidal cells. Yet, spines were present only after the first or second dendritic bifurcation. The spindle cell had only 3 primary dendrites and a ratio between primary dendrites and the number of dendritic endpoints of 1:13.6. The total length of the dendritic domain was estimated to be 8.7mm. A single apical dendrite extended into layer II and layer I where it branched extensively. The two basal dendrites extended towards the subiculum.

6.1.4 Layer V/VI

The principal neurons of EC layer V and layer VI are pyramidal cells with an average of 5.4 primary dendrites (min. 3, max. 7) and an average ratio between primary dendrites and the number of dendritic endpoints of 1:5.6 (min. 1:4, max. 1:8.7). This ratio is significantly lower compared to the ratios of neurons in the upper layers [39]. The basal dendrites distribute horizontally in layer V and layer VI where they branch sparsely or not at all. In one cell the basal dendrites extended into layer IV. The apical dendrites either bifurcate in layer IV and deep layer III or they bifurcate in layer III. In the former case the dendrites branch extensively in layer IIa and layer I. In the latter case the dendrites branch only sparsely until they reach layer I. Spines were present on all segments of the dendritic domain. The average dendritic length was estimated to be 6.2mm (min. 4.8mm, max. 7.2mm) [39, 54]. Axonal branches were evenly distributed in layer V (66.1%) as well as in layer III (33.3%) [54].

6.1.5 Interneurons

In a recent publication Buetfering et al. [6] were able to shed some light on the properties of interneurons in layer II of the MEA with the help of optogenetics. They used an adeno-associated virus to deliver and selectively incorporate channelrhodopsin-2, i.e., a light-activated ion channel into approximately 50% of the population of GABAergic⁷ interneurons in the MEA of mice. This enables the external activation of the interneurons by locally applying pulses of blue laser light through an optic fiber implanted parallel to the common set of tetrodes used for recording the electrical activity of the neurons.

The targeted interneurons control the activity of principal neurons in layer II by local GABAergic connections. The axons of the interneurons extend and branch widely within layer II where they form basket-like complexes around other neurons. Their dendritic trees are mainly located in layer I and only sparsely covered with spines receiving excitatory (fast AMPA-mediated and slow NMDA-mediated) as well as inhibitory (GABAergic) input [27]. A part of this input comes from grid cells with various phases. As a consequence the firing pattern of interneurons is not grid-like. Like many other cells of the MEA the firing rate of interneurons is modulated by running speed [6].

Collective activation of the interneurons via the light-activated ion channels silenced neurons of all cell types reliably. The delay ($< 5\text{ms}$) between the onset of

⁷inhibitory

the laser pulse and the following inhibition of postsynaptic cells is indicative of a monosynaptic connection between interneurons and principal cells. The recovery of inhibited, postsynaptic cells after the laser was switched off took 25ms. This duration is consistent with the dynamic properties of GABA_A receptors [6].

Based on their results Buetfering et al. [6] speculate that interneurons may control the gain of the grid cells rather than being essential for the generation of the grid pattern.

6.2 Topographical Organization and Microcircuits

The topographical and modular organization (section 4) of grid cells on a functional level raises the question whether this organization is reflected in the underlying neuronal structure. Within the last three decades a number of studies [35, 24, 39, 23, 71, 17, 54, 8, 4, 7, 20] have identified several anatomical properties of neurons in the MEA that exhibit a dorsoventral gradient and/or a modular organization. However, it is yet unknown if these anatomical properties are causally related to the observed functional organization of grid cells [7]. A very recent study by Gu et al. [20] provides first tentative evidence that grid cells with similar grid phases form local clusters in the MEC that are arranged in a noisy two-dimensional lattice.

Many of the anatomical properties reported below were identified by histochemical methods, i.e., the selective staining of cell parts by exploiting unique chemical properties of those parts [36]. This includes direct binding of dyes to negatively charged nucleic acids (e.g., Nissl staining using cresyl violet [8]), incorporating dyes in the process of enzyme catalysis (e.g., cytochrome oxidase [73, 23, 8]), or utilizing the selectivity of exogenous antibodies towards antigens present in the cells (e.g., reelin immunoreactivity [7]).

The layers of the MEA contain regularly distributed clusters of neurons, which are sometimes referred to as *islands*. Staining for the enzymes glycogen phosphorylase and cytochrome oxidase reveals these clusters in layer I and layer III as well as in layer II (fig. 12), respectively. Both enzymes are part of metabolic processes and the intensity of the resulting stain reflects the metabolic activity in the particular region [23, 8, 7]. The presence of cell clusters in layer II is also indicated by staining for myelin (fig. 13) [8] and by staining for immunoreactivity to the calcium-binding phosphoprotein R2D5. In the latter case layer III cells are predominantly R2D5 positive while layer II cells are R2D5 negative resulting in a pattern of interweaved, separate columns [24]. Within these columns the dendritic fields of layer II and layer III neurons receive separate projections from different brain areas [23]. The cell clusters in layer II are locally uniform in size and are surrounded by myelinated fibers. Along the dorsoventral axis the average size of the clusters increases while the average cell size and the degree of myelination decreases. Adjacent to these cell clusters lies a series of larger clusters along the dorsal and medial borders of the MEA (fig. 12 and 13) [8].

The variation of cluster size, cell size, and degree of myelination along the dorsoventral axis is accompanied by further variations on the level of individual cell properties. Garden et al. [17] studied these variations in MEA layer II stellate cells in detail. Morphologically layer II stellate cells show a dorsoventral decrease in cell body perimeter, cell body cross sectional area, and dendritic surface area. The latter is not caused by any changes to the surface area of individual dendritic

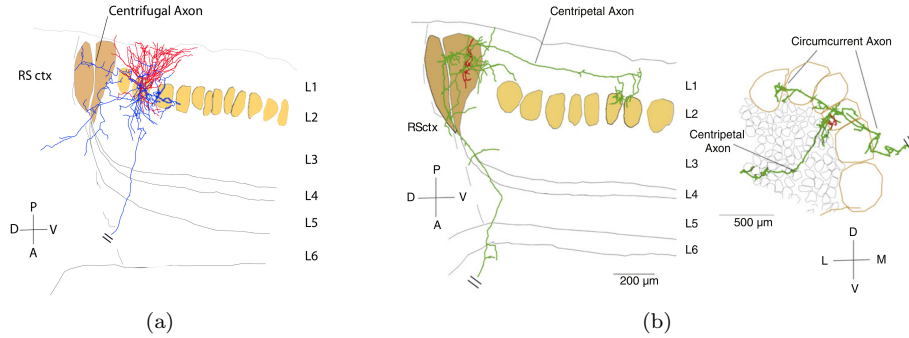


Figure 12: Two reconstructions of neuronal morphologies in the MEA. **(a)** Reconstruction of axons (blue) and dendrites (red) of a layer II stellate cell. Light brown regions indicate small layer II patches of cytochrome oxidase activity. Dark brown regions indicate large patches of cytochrome oxidase activity at the border of the MEA. D: dorsal, V: ventral, P: posterior, A: anterior, RS ctx: retrosplenial cortex. **(b)** Reconstruction of axons (green) and dendrites (red) of a cell located in a border patch identified by cytochrome oxidase activity. Left: parasagittal section, right: tangential section. L: lateral, M: medial, other labels as in (a). Figure adapted from Burgalossi et al. [8].

branches, but by an overall reduction in the number of primary dendrites from an average of ten primary dendrites at the dorsal pole to an average of seven primary dendrites at more ventral locations (fig. 14). Furthermore, the total number of dendritic branch points also decreases dorsoventrally. In addition to these morphological changes the electrotonic properties of layer II stellate cells change too along the dorsoventral axis. In particular, the input resistance and the membrane time constant increase dorsoventrally. As a consequence the current threshold to trigger action potentials (APs) decreases 4-fold along the dorsoventral axis, i.e., the amplitude of positive current required to trigger an AP is much larger at dorsal neuron locations. Moreover, the time window for the detection of coincident inputs also varies in dorsoventral direction. It is about three times wider in the most ventral locations than it is in the most dorsal ones.

Information about the microcircuitry within the EC is incomplete and commonly based just on information about the coarse morphology of principal neurons. Potential connections between neurons are often extrapolated based on overlapping input and output regions which are deduced from the neurons' dendritic and axonal domains. Although such piecewise and tentative information does only provide limited insight into the actual neuronal circuitry it does provide a set of constraints to which possible models and explanations of grid cell behavior have to adhere. To this end, the following paragraphs summarize the available, but rather fragmentary information about EC microcircuitry.

The intra-EC projections of principal neurons can be described by their horizontal extent parallel to the layers of the EC and their longitudinal extent in the orthogonal direction. In general, neurons in layer III are more restricted in their horizontal and longitudinal extent than neurons in layer II. Together they are both more restricted in their extent than neurons in layers IV to VI [35]. In

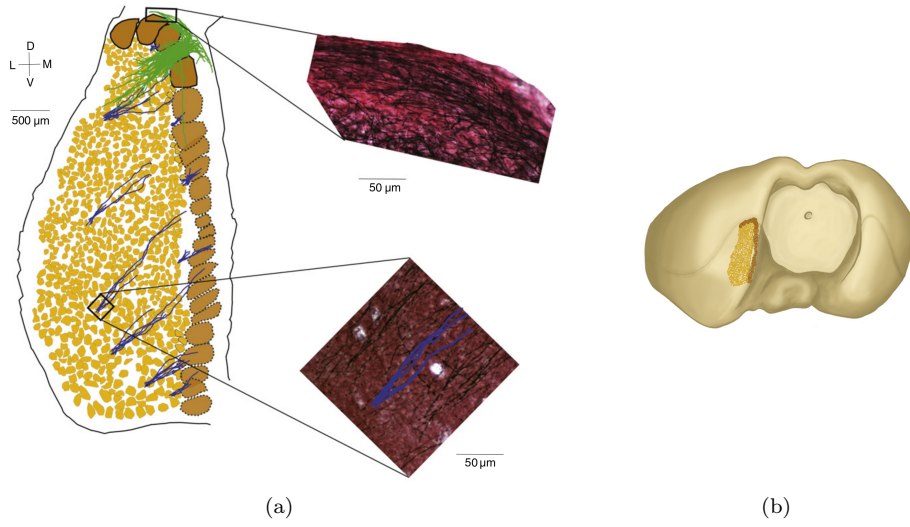


Figure 13: Large-scale overview of MEA layer I axons. **(a)** Reconstruction of MEA based on tangential sections. The sections were stained for myelin. Light brown patches are cell clusters in layer II identified in the sections as clusters of white somata surrounded by myelin. Dark brown patches are identified indirectly by extensive axon bundles on the dorsal surface of each patch. Bundles of putative centrifugal axons (blue) densely populate layer I with about twice as many bundles as small patches. Axons of cells within one large patch are drawn in green. D: dorsal, V: ventral, L: lateral, M: medial. **(b)**. Reconstruction of the MEA patches superimposed on a posteriorlateral view of the rat brain. Figure adapted from Buralossi et al. [8].

all layers, the majority of projections are oriented longitudinally and distribute between the respective layer of origin and the layers above, i.e., cells in layer V project to layers V, IV, and III; cells in layer III project to layers III, II, and I; and cells in layer II project within layer II as well as adjacent parts of layers I and III [71]. In addition, minor projections in the opposite direction were also observed, i.e., from layer II cells to layers IV, V, and VI [30, 71]; and from layer III cells to layer V [54]. By comparison layer V neurons contribute three times more intrinsic connections than neurons in layer II and five times more than neurons in layer III. The axonal arbor of layer V neurons is cone shaped with its base in layer V and its peak in layer II. This suggests that layer V cells predominantly interact with each other via their basal dendrites. In contrast, the axonal domain of layer II neurons forms an inverted cone with its base in layer I and its peak between layers III and V. This allows layer II cells to communicate with a wide range of neurons in layers II, III, and V. Layer III neurons may represent some form of bidirectional link between deep and superficial layers as they can receive input from all layers and possess axons that converge on smaller subsets of layer II and/or layer V cells [54]. Local excitatory connections between principal cells were observed in layer III [70, 71] and layer V [71], but none [71, 7] or few [54] in layer II. The latter results are called into question in a recent study by Winterer et al. [70] who measured (in vitro) intra-layer

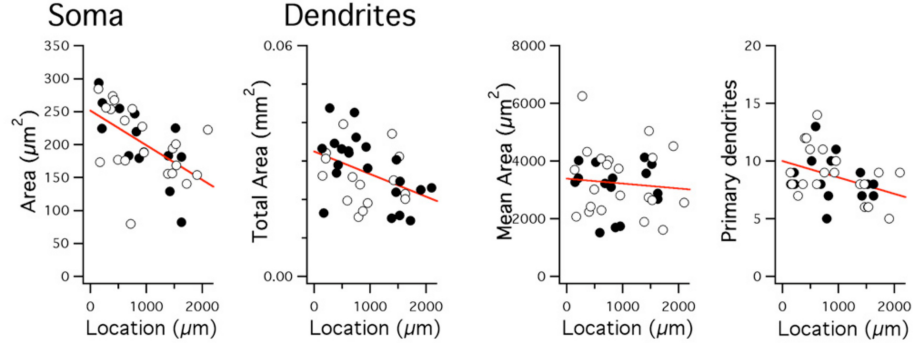


Figure 14: Variation of morphological properties of MEA layer II stellate cells along the dorsoventral axis. The plots show (from left to right) the cross sectional soma area, total dendritic surface area, average dendritic surface area, and number of primary dendrites of reconstructed stellate cells plotted against the soma’s distance from the dorsal pole. Open and closed circles refer to two different recording conditions used to measure the cell’s electrotonic properties. Both conditions did not influence the measurement of the morphological properties shown here. Figure adapted from Garden et al. [17].

excitatory connections between layer II stellate cells at a rate of 2.5%. In the same study Winterer et al. also report on predominantly unidirectional excitatory connections between layer II/III pyramidal cells and layer II stellate cells (13.5% and 7.0%, respectively).

Neurons in the larger clusters at the EC border are targeted by axons of layer II stellate cells (fig. 12a) as well as layer III pyramidal cells. The so called *centrifugal axons* appear to be bundled and oriented in dorsomedial direction (fig. 13a). The targeted cells in the large clusters differ in their morphology from all other neurons in the MEA. Their dendritic trees are small and extend not beyond their home cluster. They possess three main axons: one axon descending towards the presubiculum, one *circumcurrent axon* targeting many other large clusters along the EC border, and one *centripetal axon* specifically targeting one to two small layer II clusters in which it arborizes. In addition, a number of axons branch locally within the home cluster (fig. 12b). The firing characteristics of large cluster cells range from spatially multi-peaked firing to spatially broad tuning, all with a high degree of modulation by head direction [8].

A more detailed view on the microcircuitry of MEA layer II was recently provided by Varga et al. [67]. They identified two major, non-overlapping cell groups in layer II by utilizing the cells’ immunoreactivity to either reelin ($53 \pm 2.6\%$ of all cells) or calbindin ($44 \pm 2.2\%$ of all cells). Only $2.8 \pm 1.1\%$ of all cells were reelin and calbindin double positive⁸. More importantly, injection of the retrograde tracer biotinylated dextrane amine (BDA) into the ipsilateral dentate gyrus labeled predominantly ($98.5 \pm 0.5\%$) the reelin positive principal cells indicating that only these cells project to the dentate gyrus. In contrast, the calbindin-expressing principal cells were found to project extra-hippocampally to the contralateral entorhinal cortex. In addition, Varga et al. were able to show

⁸Total number of cells analyzed in 3 rats: 1152

that reelin positive and calbindin positive cells each interact with a different population of inhibitory interneurons. Reelin-expressing principal cells interact with fast-spiking interneurons, whereas calbindin-expressing cells interact with interneurons that form basket-like axonal domains surrounding the principle cells providing perisomatic inhibition. The observations of Varga et al. are confirmed by a more recent study by Ray et al. [55]. In addition, Ray et al. were able to show that calbindin negative cells were primarily stellate cells whereas calbindin positive cells were primarily pyramidal cells. The latter were observed to form hexagonal patches near the layer I/II border. This hexagonal structure led Ray et al. to hypothesize that the cells' arrangement "might be an isomorphism to hexagonal grid activity". However, they were not able to measure the spatial modulation in a sufficient number of identified cells to assess the validity of this hypothesis. In a related study Tang et al. [63] were able to find potential evidence that grid cells are "preferentially recruited" from the population of calbindin positive cells, i.e., pyramidal cells, and that border cells stem preferentially from calbindin negative cells, i.e., stellate cells.

Regarding projections into the EC Lingenhöhl and Finch [39] as well as Bonnevie et al. [4] could make interesting, and to some degree contradicting observations. Lingenhöhl and Finch [39] investigated projections from the hippocampal area to the EC in vitro. In response to electrical stimulation of either the DG, CA1 or CA3 all cells that were observed in the EC showed synaptic responses in form of inhibitory postsynaptic potentials (IPSPs). No clear excitatory postsynaptic potentials (EPSPs) could be identified indicating that projections from hippocampal areas to the EC are predominantly inhibitory. However, Bonnevie et al. [4] investigated projections from the hippocampus to the MEA in vivo on a functional level. They observed grid cells in the MEA before and after the inactivation of the hippocampus. In the latter case grid cells lost their grid-like firing pattern and became direction sensitive. Based on these results Bonnevie et al. concluded that grid cells require excitatory drive from the hippocampus. The results of Lingenhöhl and Finch and Bonnevie et al. do not necessarily contradict each other. The postulated excitatory drive could reach the EC on an indirect route, e.g., via the subiculum or the pre- and parasubiculum.

7 Conclusions

Since their discovery a decade ago grid cells have attracted considerable attention resulting in a better and more detailed understanding of their functional characteristics as well as a better understanding of the parahippocampal-hippocampal region they embedded in. The observation of new grid cell phenomena like the strong influence of environmental geometry or the fragmentation of grid patterns question early hypothesis on grid cell function and call for revised models of grid cell behavior that allow to formulate new hypothesis and direct further experimental investigation. Considering the presence of related cell types like border cells, head direction cells, irregular spatial cells, and non-spatial cells that all converge on hippocampal neurons and may receive feedback from these in turn, it appears essential that new models should aim to integrate these different types of signals into a single, conceptual framework that explains the processing of information within a wider context that extends beyond isolated descriptions

of individual cell types and their behavior.

References

- [1] Caswell Barry, Lin Lin Ginzberg, John O’Keefe, and Neil Burgess. Grid cell firing patterns signal environmental novelty by expansion. *Proceedings of the National Academy of Sciences*, 109(43):17687–17692, 2012.
- [2] Caswell Barry, Robin Hayman, Neil Burgess, and Kathryn J. Jeffery. Experience-dependent rescaling of entorhinal grids. *Nat Neurosci*, 10(6):682–684, jun 2007.
- [3] Charlotte N Boccara, Francesca Sargolini, Veslemoy Hult Thoresen, Trygve Solstad, Menno P Witter, Edvard I Moser, and May-Britt Moser. Grid cells in pre- and parasubiculum. *Nat Neurosci*, 13(8):987–994, August 2010.
- [4] Tora Bonnevie, Benjamin Dunn, Marianne Fyhn, Torkel Hafting, Dori Derdikman, John L Kubie, Yasser Roudi, Edvard I Moser, and May-Britt Moser. Grid cells require excitatory drive from the hippocampus. *Nat Neurosci*, 16(3):309–317, March 2013.
- [5] Vegard Heimly Brun, Trygve Solstad, Kirsten Brun Kjelstrup, Marianne Fyhn, Menno P. Witter, Edvard I. Moser, and May-Britt Moser. Progressive increase in grid scale from dorsal to ventral medial entorhinal cortex. *Hippocampus*, 18(12):1200–1212, 2008.
- [6] Christina Buetfering, Kevin Allen, and Hannah Monyer. Parvalbumin interneurons provide grid cell-driven recurrent inhibition in the medial entorhinal cortex. *Nat Neurosci*, 17(5):710–718, 5 2014.
- [7] Andrea Burgalossi and Michael Brecht. Cellular, columnar and modular organization of spatial representations in medial entorhinal cortex. *Current Opinion in Neurobiology*, 24(0):47 – 54, 2014.
- [8] Andrea Burgalossi, Lucas Herfst, Moritz von Heimendahl, Henning Förste, Kurt Haskic, Martin Schmidt, and Michael Brecht. Microcircuits of functionally identified neurons in the rat medial entorhinal cortex. *Neuron*, 70(4):773–786, May 2011.
- [9] Francis Carpenter and Caswell Barry. Distorted grids as a spatial label and metric. *Trends in Cognitive Sciences*, 20(3):164 – 167, 2016.
- [10] Francis Carpenter, Daniel Manson, Kate Jeffery, Neil Burgess, and Caswell Barry. Grid cells form a global representation of connected environments. *Current Biology*, pages 1176–1182, 2015.
- [11] Dori Derdikman, Jonathan R. Whitlock, Albert Tsao, Marianne Fyhn, Torkel Hafting, May-Britt Moser, and Edvard I. Moser. Fragmentation of grid cell maps in a multicompartiment environment. *Nat Neurosci*, 12(10):1325–1332, October 2009.

- [12] Geoffrey W. Diehl, Olivia J. Hon, Stefan Leutgeb, and Jill K. Leutgeb. Grid and nongrid cells in medial entorhinal cortex represent spatial location and environmental features with complementary coding schemes. *Neuron*, 94(1):83 – 92.e6, 2017.
- [13] Geoffrey W. Diehl, Olivia J. Hon, Stefan Leutgeb, and Jill K. Leutgeb. Stability of medial entorhinal cortex representations over time. *Hippocampus*, pages 1 – 19, 2018.
- [14] Mark C. Fuhs and David S. Touretzky. A spin glass model of path integration in rat medial entorhinal cortex. *The Journal of Neuroscience*, 26(16):4266–4276, 2006.
- [15] Marianne Fyhn, Torkel Hafting, Alessandro Treves, May-Britt Moser, and Edvard I. Moser. Hippocampal remapping and grid realignment in entorhinal cortex. *Nature*, 446(7132):190–194, March 2007.
- [16] Marianne Fyhn, Sturla Molden, Menno P. Witter, Edvard I. Moser, and May-Britt Moser. Spatial representation in the entorhinal cortex. *Science*, 305(5688):1258–1264, 2004.
- [17] Derek L.F. Garden, Paul D. Dodson, Cian O’Donnell, Melanie D. White, and Matthew F. Nolan. Tuning of synaptic integration in the medial entorhinal cortex to the organization of grid cell firing fields. *Neuron*, 60(5):875–889, 2008.
- [18] P. Germroth, W.K. Schwerdtfeger, and E.H. Buhl. Morphology of identified entorhinal neurons projecting to the hippocampus. a light microscopical study combining retrograde tracing and intracellular injection. *Neuroscience*, 30(3):683 – 691, 1989.
- [19] Lisa M. Giocomo, May-Britt Moser, and Edvard I. Moser. Computational models of grid cells. *Neuron*, 71(4):589 – 603, 2011.
- [20] Yi Gu, Sam Lewallen, Amina A. Kinkhabwala, Cristina Domnisoru, Kijung Yoon, Jeffrey L. Gauthier, Ila R. Fiete, and David W. Tank. A map-like micro-organization of grid cells in the medial entorhinal cortex. *Cell*, 2018.
- [21] Torkel Hafting, Marianne Fyhn, Tora Bonnevie, May-Britt Moser, and Edvard I. Moser. Hippocampus-independent phase precession in entorhinal grid cells. *Nature*, 453(7199):1248–1252, June 2008.
- [22] Torkel Hafting, Marianne Fyhn, Sturla Molden, May-Britt Moser, and Edvard I. Moser. Microstructure of a spatial map in the entorhinal cortex. *Nature*, 436(7052):801–806, August 2005.
- [23] R F Hevner and M T Wong-Riley. Entorhinal cortex of the human, monkey, and rat: metabolic map as revealed by cytochrome oxidase. *J Comp Neurol*, 326(3):451–469, 1992.
- [24] J. Ikeda, K. Mori, S. Oka, and Y. Watanabe. A columnar arrangement of dendritic processes of entorhinal cortex neurons revealed by a monoclonal antibody. *Brain Research*, 505:176–179, 1989.

- [25] Ricardo Insausti. Comparative anatomy of the entorhinal cortex and hippocampus in mammals. *Hippocampus*, 3(S1):19–26, 1993.
- [26] Karel Jezek, Espen J. Henriksen, Alessandro Treves, Edvard I. Moser, and May-Britt Moser. Theta-paced flickering between place-cell maps in the hippocampus. *Nature*, 478(7368):246–249, October 2011.
- [27] R.S.G. Jones and E.H. Bühl. Basket-like interneurons in layer {II} of the entorhinal cortex exhibit a powerful nmda-mediated synaptic excitation. *Neuroscience Letters*, 149(1):35 – 39, 1993.
- [28] Jochen Kerdels. *A Computational Model of Grid Cells based on a Recursive Growing Neural Gas*. PhD thesis, Hagen, 2016.
- [29] Kirsten Brun Kjelstrup, Trygve Solstad, Vegard Heimly Brun, Torkel Hafting, Stefan Leutgeb, Menno P. Witter, Edvard I. Moser, and May-Britt Moser. Finite scale of spatial representation in the hippocampus. *Science*, 321(5885):140–143, 2008.
- [30] Ruby Klink and Angel Alonso. Morphological characteristics of layer ii projection neurons in the rat medial entorhinal cortex. *Hippocampus*, 7(5):571–583, 1997.
- [31] Benjamin J. Kraus, Mark P. Brandon, Robert J. Robinson II, Michael A. Connerney, Michael E. Hasselmo, and Howard Eichenbaum. During running in place, grid cells integrate elapsed time and distance run. *Neuron*, 88(3):578 – 589, 2015.
- [32] Emilio Kropff, James E. Carmichael, May-Britt Moser, and Edvard I. Moser. Speed cells in the medial entorhinal cortex. *Nature*, 523(7561):419–424, July 2015.
- [33] Julija Krupic, Marius Bauza, Stephen Burton, Caswell Barry, and John O’Keefe. Grid cell symmetry is shaped by environmental geometry. *Nature*, 518(7538):232–235, February 2015.
- [34] Julija Krupic, Neil Burgess, and John O’Keefe. Neural representations of location composed of spatially periodic bands. *Science*, 337(6096):853–857, 2012.
- [35] C Köhler. Intrinsic connections of the retrohippocampal region in the rat brain. ii. the medial entorhinal area. *J Comp Neurol*, 246(2):149–169, 1986.
- [36] G. Lang. *Histotechnik*. SpringerLink : Bücher. Springer, 2013.
- [37] Rosamund F. Langston, James A. Ainge, Jonathan J. Couey, Cathrin B. Canto, Tale L. Bjerknes, Menno P. Witter, Edvard I. Moser, and May-Britt Moser. Development of the spatial representation system in the rat. *Science*, 328(5985):1576–1580, 2010.
- [38] Stefan Leutgeb, Jill K. Leutgeb, Carol A. Barnes, Edvard I. Moser, Bruce L. McNaughton, and May-Britt Moser. Independent codes for spatial and episodic memory in hippocampal neuronal ensembles. *Science*, 309(5734):619–623, 2005.

- [39] K. Lingenhöhl and D.M. Finch. Morphological characterization of rat entorhinal neurons in vivo: soma-dendritic structure and axonal domains. *Experimental Brain Research*, 84(1):57–74, 1991.
- [40] Elizabeth Marozzi, Lin Lin Ginzberg, Andrea Alenda, and Kate J. Jeffery. Purely translational realignment in grid cell firing patterns following nonmetric context change. *Cerebral Cortex*, 2015.
- [41] Patrick D. Martin and Alain Berthoz. Development of spatial firing in the hippocampus of young rats. *Hippocampus*, 12(4):465–480, 2002.
- [42] Bruce L. McNaughton, Francesco P. Battaglia, Ole Jensen, Edvard I Moser, and May-Britt Moser. Path integration and the neural basis of the ‘cognitive map’. *Nat Rev Neurosci*, 7(8):663–678, August 2006.
- [43] Chenglin Miao, Qichen Cao, Hiroshi T. Ito, Homare Yamahachi, Menno P. Witter, May-Britt Moser, and Edvard I. Moser. Hippocampal remapping after partial inactivation of the medial entorhinal cortex. *Neuron*, 88(3):590 – 603, 2015.
- [44] Joseph D. Monaco and Larry F. Abbott. Modular realignment of entorhinal grid cell activity as a basis for hippocampal remapping. *The Journal of Neuroscience*, 31(25):9414–9425, 2011.
- [45] Edvard I. Moser, Emilio Kropff, and May-Britt Moser. Place cells, grid cells, and the brain’s spatial representation system. *Annual Review of Neuroscience*, 31:69–89, 2008.
- [46] Edvard I. Moser and May-Britt Moser. A metric for space. *Hippocampus*, 18(12):1142–1156, 2008.
- [47] Edvard I. Moser, Yasser Roudi, Menno P. Witter, Clifford Kentros, Tobias Bonhoeffer, and May-Britt Moser. Grid cells and cortical representation. *Nat Rev Neurosci*, 15(7):466–481, July 2014.
- [48] RU Muller and JL Kubie. The effects of changes in the environment on the spatial firing of hippocampal complex-spike cells. *The Journal of Neuroscience*, 7(7):1951–1968, 1987.
- [49] J. O’Keefe and D.H. Conway. Hippocampal place units in the freely moving rat: Why they fire where they fire. *Experimental Brain Research*, 31(4):573–590, 1978.
- [50] J. O’Keefe and J. Dostrovsky. The hippocampus as a spatial map. preliminary evidence from unit activity in the freely-moving rat. *Brain Research*, 34(1):171 – 175, 1971.
- [51] John O’Keefe. Place units in the hippocampus of the freely moving rat. *Experimental Neurology*, 51(1):78 – 109, 1976.
- [52] John O’Keefe and Michael L. Recce. Phase relationship between hippocampal place units and the EEG theta rhythm. *Hippocampus*, 3(3):317–330, 1993.

- [53] H Freyja Olafsdottir, Francis Carpenter, and Caswell Barry. Coordinated grid and place cell replay during rest. *Nat Neurosci*, advance online publication:–, April 2016.
- [54] Pascale Quilichini, Anton Sirota, and György Buzsáki. Intrinsic circuit organization and theta–gamma oscillation dynamics in the entorhinal cortex of the rat. *The Journal of Neuroscience*, 30(33):11128–11142, 2010.
- [55] Saikat Ray, Robert Naumann, Andrea Burgalossi, Qiusong Tang, Helene Schmidt, and Michael Brecht. Grid-layout and theta-modulation of layer 2 pyramidal neurons in medial entorhinal cortex. *Science*, 343(6173):891–896, 2014.
- [56] David Rowland, Horst A Obenhaus, Emilie R Skytøen, Qiangwei Zhang, Cliff G Kentros, Edvard I Moser, and May-Britt Moser. Functional properties of stellate cells in medial entorhinal cortex layer ii. *eLife*, 7, 09 2018.
- [57] Jon W. Rueckemann, Audrey J. DiMauro, Lara M. Rangel, Xue Han, Edward S. Boyden, and Howard Eichenbaum. Transient optogenetic inactivation of the medial entorhinal cortex biases the active population of hippocampal neurons. *Hippocampus*, 26(2):246–260, 2016.
- [58] Francesca Sargolini, Marianne Fyhn, Torkel Hafting, Bruce L. McNaughton, Menno P. Witter, May-Britt Moser, and Edvard I. Moser. Conjunctive representation of position, direction, and velocity in entorhinal cortex. *Science*, 312(5774):758–762, 2006.
- [59] Francesco Savelli, D. Yoganarasimha, and James J. Knierim. Influence of boundary removal on the spatial representations of the medial entorhinal cortex. *Hippocampus*, 18(12):1270–1282, 2008.
- [60] Trygve Solstad, Charlotte N. Boccara, Emilio Kropff, May-Britt Moser, and Edvard I. Moser. Representation of geometric borders in the entorhinal cortex. *Science*, 322(5909):1865–1868, 2008.
- [61] Hanne Stensola, Tor Stensola, Trygve Solstad, Kristian Froland, May-Britt Moser, and Edvard I. Moser. The entorhinal grid map is discretized. *Nature*, 492(7427):72–78, December 2012.
- [62] Tor Stensola, Hanne Stensola, May-Britt Moser, and Edvard I. Moser. Shearing-induced asymmetry in entorhinal grid cells. *Nature*, 518(7538):207–212, February 2015.
- [63] Qiusong Tang, Andrea Burgalossi, ChristianÂ Laut Ebbesen, Saikat Ray, Robert Naumann, Helene Schmidt, Dominik Spicher, and Michael Brecht. Pyramidal and stellate cell specificity of grid and border representations in layer 2 of medial entorhinal cortex. *Neuron*, 84(6):1191–1197, 2014.
- [64] Qiusong Tang, Christian L. Ebbesen, Juan I. Sanguinetti-Scheck, Patricia Preston-Ferrer, Anja Gundlfinger, Jochen Winterer, Prateep Beed, Saikat Ray, Robert Naumann, Dietmar Schmitz, Michael Brecht, and Andrea Burgalossi. Anatomical organization and spatiotemporal firing patterns of layer 3 neurons in the rat medial entorhinal cortex. *The Journal of Neuroscience*, 35(36):12346–12354, September 2015.

- [65] JS Taube. Head direction cells recorded in the anterior thalamic nuclei of freely moving rats. *The Journal of Neuroscience*, 15(1):70–86, 1995.
- [66] JS Taube, RU Muller, and JB Ranck. Head-direction cells recorded from the postsubiculum in freely moving rats. i. description and quantitative analysis. *The Journal of Neuroscience*, 10(2):420–435, 1990.
- [67] Csaba Varga, Soo Yeun Lee, and Ivan Soltesz. Target-selective gabaergic control of entorhinal cortex output. *Nat Neurosci*, 13(7):822–824, July 2010.
- [68] Tanja Wernle, Torgeir Waaga, Maria MÅrreaunet, Alessandro Treves, May-Britt Moser, and Edvard I. Moser. Integration of grid maps in merged environments. *Nature Neuroscience*, December 2017.
- [69] Tom J. Wills, Francesca Cacucci, Neil Burgess, and John O’Keefe. Development of the hippocampal cognitive map in preweanling rats. *Science*, 328(5985):1573–1576, 2010.
- [70] Jochen Winterer, Nikolaus Maier, Christian Wozny, Prateep Beed, Jörg Breustedt, Roberta Evangelista, Yangfan Peng, Tiziano D’Albis, Richard Kempter, and Dietmar Schmitz. Excitatory microcircuits within superficial layers of the medial entorhinal cortex. *Cell Reports*, 19(6):1110–1116, 2017.
- [71] Menno P. Witter and Edvard I. Moser. Spatial representation and the architecture of the entorhinal cortex, December 2006.
- [72] Menno P. Witter, Pieterke A. Naber, Theo van Haeften, Willem C.M. Machielsen, Serge A.R.B. Rombouts, Frederik Barkhof, Philip Scheltens, and Fernando H. Lopes da Silva. Cortico-hippocampal communication by way of parallel parahippocampal-subicular pathways. *Hippocampus*, 10(4):398–410, 2000.
- [73] Margaret T.T. Wong-Riley. Cytochrome oxidase: an endogenous metabolic marker for neuronal activity. *Trends in Neurosciences*, 12(3):94 – 101, 1989.
- [74] Michael M. Yartsev, Menno P. Witter, and Nachum Ulanovsky. Grid cells without theta oscillations in the entorhinal cortex of bats. *Nature*, 479(7371):103–107, November 2011.
- [75] KiJung Yoon, Michael A Buice, Caswell Barry, Robin Hayman, Neil Burgess, and Ila R Fiete. Specific evidence of low-dimensional continuous attractor dynamics in grid cells. *Nat Neurosci*, 16(8):1077–1084, August 2013.
- [76] Sheng-Jia Zhang, Jing Ye, Chenglin Miao, Albert Tsao, Ignas Cerniauskas, Debora Ledergerber, May-Britt Moser, and Edvard I. Moser. Optogenetic dissection of entorhinal-hippocampal functional connectivity. *Science*, 340(6128), 2013.